Photothermal Therapy

International Edition: DOI: 10.1002/anie.201510597
German Edition: DOI: 10.1002/ange.201510597

Degradable Molybdenum Oxide Nanosheets with Rapid Clearance and Efficient Tumor Homing Capabilities as a Therapeutic Nanoplatform

Guosheng Song, Jiali Hao, Chao Liang, Teng Liu, Min Gao, Liang Cheng, Junqing Hu, and Zhuang Liu**

Abstract: *Molybdenum oxide (MoOx) nanosheets with high near-infrared (NIR) absorbance and pH-dependent oxidative degradation properties were synthesized, functionalized with polyethylene glycol (PEG), and then used as a degradable photothermal agent and drug carrier. The nanosheets, which are relatively stable under acidic pH, could be degraded at physiological pH. Therefore, MoOx-PEG distributed in organs upon intravenous injection would be rapidly degraded and excreted without apparent in vivo toxicity. MoOx-PEG shows efficient accumulation in tumors, the acidic pH of which then leads to longer tumor retention of those nanosheets. Along with the capability of acting as a photothermal agent for effective tumor ablation, MoOx-PEG can load therapeutic molecules with high efficiencies. This concept of inorganic theranostic nanoagent should be relatively stable in tumors to allow imaging and treatment, while being readily degradable in normal organs to enable rapid excretion and avoid long-term retention/toxicity.*

Inorganic nanomaterials with many intriguing physical and chemical properties have shown great promise for cancer imaging and therapy.[1] Various inorganic nanoparticles with interesting magnetic and/ or optical properties have been extensively explored as nanoprobes for biomedical detection and imaging.[2] As far as therapeutic nanoparticles are concerned, inorganic nanoparticles have also presented significant potential, acting either as drug delivery carriers,[3] or as therapeutic agents by themselves (such as photothermal therapy or magnetic hyperthemia).[1,4] Those nanoparticles often could passively accumulate in tumors with higher concentrations and longer retention time compared to small molecules via the enhanced permeability and retention (EPR) effect, endowing their abilities to address many challenges that can hardly be achieved by small molecular drugs.[5] The inherent physical properties of inorganic nanoagents in many cases also cannot be easily matched by small organic molecules.[5c] However, unlike small molecules which usually could be rapidly excreted from the body after systemic administration, inorganic nanoparticles with relatively large sizes (for example, hydrodynamic diameters larger than 6–8 nm) would accumulate in reticuloendothelial systems (RES) such as liver and spleen for long periods of time.[6] Without efficient clearance, the potential long-term toxicity of those inorganic nanomaterials could be a serious concern that hampers their further clinical use.[7]

Recently, substantial efforts have been devoted to the development of functional inorganic nanomaterials that can be quickly excreted upon systemic administration.[5c,6,8] The main strategy is to synthesize ultrasmall nanoparticles and functionalize them with a thin layer of hydrophilic coating, so as to minimize their hydrodynamic sizes in the physiological environment to enable rapid renal filtration.[5c,6,8] However, those ultra-small nanoparticles would behave somewhat like small molecules: their rapid renal excretion on the other hand would lead to the shortened blood circulation half-lives and weakened EPR effect, resulting in reduced tumor accumulation and retention.[5c,6] Ideally, it would be the best to develop inorganic nanoagents which can be quickly excreted from the normal organs of the body, while being able to effectively accumulate and retain in tumors, upon systemic administration.

With rapid cell growth and insufficient blood supply, the tumor microenvironment is known to be more acidic and hypoxic than normal tissues.[9] Taking advantages of such differences between tumor microenvironment and normal physiological conditions, PEGylated molybdenum oxide nanosheets (MoOx-PEG) with pH-dependent degradation properties are synthesized and rationally used as a degradable inorganic therapeutic agent. Those MoOx-PEG nanosheets are relatively stable under the acidic pH, but could be quickly degraded under the physiological pH. On one hand, MoOx-PEG could be rapidly excreted from the body after intravenous injection without long-time retention in RES organs of mice. On the other hand, such MoOx-PEG still shows efficiently accumulation and a long period of retention in the tumor via the EPR effect. Employing the strong NIR absorbance of those nanosheets, effective NIR-triggered photothermal ablation of tumors could be realized afterwards. Furthermore, the ultra-high specific surface area of those MoOx-PEG nanosheets allows efficient loading of therapeutic molecules on their surface, enabling their applications in drug delivery and potentially combination cancer therapy. Our work thus develops a new type of multifunctional 2D nano-agent, which shows capabilities of rapid excretion together with efficient tumor homing and retention.

[*] Dr. G. Song, J. Hao, C. Liang, T. Liu, M. Gao, Prof. L. Cheng, Prof. Z. Liu
Institute of Functional Nano & Soft Materials (FUNSOM), Collaborative Innovation Center of Suzhou Nano Science and Technology, Soochow University Suzhou
Jiangsu 215123 (China)
E-mail: zliu@suda.edu.cn
Prof. J. Hu
College of Materials Science and Engineering, Donghua University
Shanghai 201620 (China)
E-mail: hu.junqing@dhu.edu.cn

Supporting information for this article is available on the WWW under http://dx.doi.org/10.1002/anie.201510597.

Molybdenum oxide nanosheets were successfully prepared by a one-pot hydrothermal method.[10] Transmission electron microscopy (TEM) and atomic force microscopy (AFM) images revealed that the obtained nanostructures showed sheet-like morphology with diameters at hundreds of nanometers (Figure 1 a). The average thickness of those nanosheets was measured to be about 1.5 nm by AFM (Figure 1 b,c).

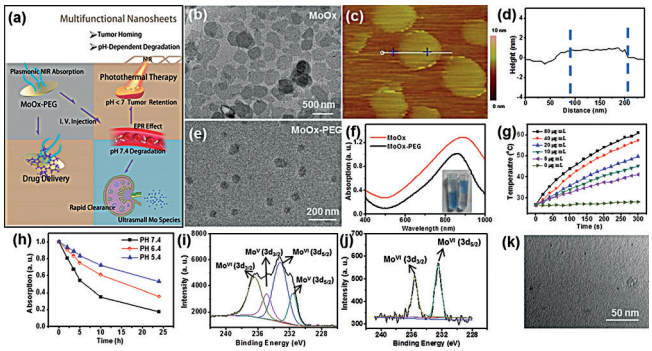

Figure 1. Synthesis and characterization of MoOx ultrathin nanosheets and MoOx-PEG. a) The use of MoOx-PEG nanosheets for photothermal therapy and drug loading, as well as their degradation and excretion. b), c) TEM (b) and AFM (c) images of as-made MoOx. d) The AFM-measured height profile of MoOx, which showed a thickness of about 1.5 nm. e) A TEM image of MoOx-PEG. f) UV/Vis-NIR absorbance spectra of MoOx and MoOx-PEG. Inset: a photograph of MoOx-PEG transferred from chloroform to water after surface modification. g) Photothermal heating curves of MoOx-PEG with different concentrations under an 808-nm laser irradiation (0.7 $W c^{-2}$). h) Degradation process of MoOx-PEG incubated in serum with different pH values (7.4, 6.4, and 5.4) over time, as measured by the UV/Vis-NIR absorption spectra. i), j) Mo 3d peaks in XPS spectra of MoOx-PEG before (i) and after (j) degradation. k) TEM image of the degradation product of MoOx-PEG.

Characterization by energy-dispersive X-ray (EDX), X-ray photoelectron (XPS), and Raman spectra showed that those nanosheets were composed by Mo, O, and possibly H elements (Supporting Information, Figure S1). Further XPS analysis of Mo^{3d} peaks revealed that those nanosheets consisted of both Mo^{V} and Mo^{VI} (Supporting Information, Figure S1c), suggesting that the Mo^{VI} precursor, ammonium molybdate, was partially reduced by oleylamine in the hydrothermal process, giving hydrogen molybdenum bronze $H_x(Mo^{V}_x)(Mo^{VI}_{1-x})O_3$ (abbreviated as MoOx) [Equation (1)].[10,11]

$$(NH_4)_6Mo^{VI}_7O_{24} + HCl \rightarrow H_6Mo^{VI}_7O_{24} \xrightarrow[heat]{NH_2C_{18}H_{35}} H_x(Mo^{V}_x)Mo^{VI}_{1-x})O_3 \quad (1)$$

To functionalize those nanosheets, as-made MoOx was modified by an amphiphilic polymer, PEG-grafted poly (maleicanhydride-alt-1-octadecene), under vigorous sonication, which would also break large nanosheets into small pieces. The obtained PEGylated MoOx (MoOx-PEG) showed reduced sizes to be about 90 nm (Figure 1 e), and could be well dispersed in various solutions, including water, phosphate-buffered saline (PBS), and cell culture medium without aggregation (Supporting Information, Figure S2). Importantly, such MoOx-PEG exhibited strong absorption from 700 to 1000 nm (Figure 1 f), which could be attributed to the localized surface plasmon resonance (LSPR) originated from the intervalence charge-transfer transition between Mo^{V} and Mo^{VI}.[10,12] The mass extinction coefficient of MoOx-PEG at 800 nm was calculated to be 37.3 $L g^{-1} cm^{-1}$, a value much higher than that of several widely explored photothermal agents, such as graphene oxide (GO) (3.6 $L g^{-1} cm^{-1}$), reduced GO (rGO) (24.6 $L g^{-1} cm^{-1}$),[13] MoS_2 (28.4 $L g^{-1} cm^{-1}$),[5b] WS_2 (23.8 $L g^{-1} cm^{-1}$) nanosheet,[14] and Au nanorods (13.9 $L g^{-1} cm^{-1}$).[13] Owing to the high NIR absorption, MoOx-PEG showed excellent photothermal effect under irradiation by an 808-nm NIR laser (Figure 1 g; Supporting Information, Figure S3).

Mo^{V} at the intermediate valence state may be oxidized into Mo^{VI} in the presence of oxygen. Under alkali conditions, MoO_3, which is colorless, may be solubilized into MoO_4^{2-} as small ions. We thus studied the stability of MoOx-PEG in serum and phosphate buffers under different pH values by measuring the LSPR absorption of those nanosheets (Figure 1 h; Supporting Information, Figures S4, S5). It was found that MoOx-PEG degraded quickly in alkali solutions (pH 9.4, 11.4) but appeared to be quite stable in acidic solutions (such as at pH 3.4 and 5.4). Under a neutral solution in serum or buffer, MoOx-PEG showed gradual degradation. Notably, the degradation of MoOx-PEG in serum appeared to be slower than that in the buffer at pH 7.4, which is most likely due to the possible formation of protein corona on the nanosheet surface to slow down their degradation. XPS spectra revealed that while there was 35 % of Mo^{V} in the initial MoOx-PEG sample (Figure 1 i), the degradation product after being incubated in PBS at pH 7.4 for 24 h contained only about 4 % of Mo^{V} and about 96 % of Mo^{VI} (Figure 1 j), indicating that most of Mo^{V} was oxidized to Mo^{VI} for those nanosheets under the physiological pH, a reason resulting in the great diminution of LSPR absorption in the NIR region. Moreover, the small-angle X-ray diffraction patterns of degradation product showed no obvious peaks (Supporting Information, Figure S6), indicating its amorphous structure. Based on TEM imaging, no large nanoparticles were seen in the degradation product, except for a few ultrasmall particles less than 5 nm (Figure 1 k), which possibly could be filtrated via the kidneys. Therefore, we propose that under the alkali condition, $H_x(Mo^{V}_x)(Mo^{VI}_{1-x})O_3$ could be firstly neutralized to the unstable intermediate product $[(Mo^{V}_x)(Mo^{VI}_{1-x})O_3]^-$, which is then oxidized into $[Mo^{VI}O_4]^{2-}$ [Equations (2) and (3)]), resulting in the decrease of the LSPR absorption peak. Under acidic conditions, however, $H_x(Mo^{V}_x)(Mo^{VI}_{1-x})O_3$ is more stable, and the oxidation of Mo^{V}_x may be slower.

$$H_x(Mo^{V}_x)(Mo^{VI}_{1-x})O_3 + OH^- \rightarrow [(Mo^{V}_x)(Mo^{VI}_{1-x})O_3]^- + H_2O \quad (2)$$

$$[(Mo^{V}_x)(Mo^{VI}_{1-x})O_3]^- + O_2 \rightarrow [Mo^{VI}O_4]^{2-} \quad (3)$$

Rapid body clearance would minimize tissue exposures to nanomaterials and thus reduce their potential long-term toxicity.[7] The clearance of MoOx-PEG was investigated by

measuring Mo contents in major organs and tissues of mice at different time points post intravenous (i.v.) injection of MoOx-PEG (20 mg kg^{-1}), using inductively-coupled plasma atomic-emission spectroscopy (ICP-AES) (Figure 2a). It was

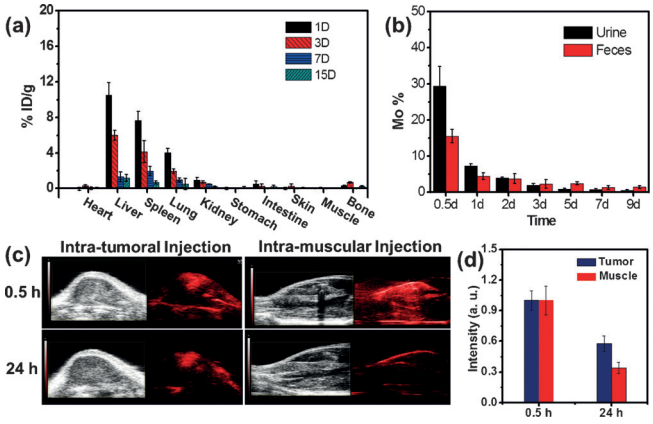

Figure 2. Biodistribution and clearance of MoOx-PEG nanosheets. a) Time-dependent biodistribution of molybdenum in female Balb/c mice after i.v. injection of MoOx-PEG. b) Molybdenum in urine and feces collected at various time points after injection. c) Ultrasound (US) and PA imaging of the tumor and muscle at 0.5 h and 24 h post injection of MoOx-PEG. d) Relative PA signal intensities at 0.5 h and 24 h post injection in the tumor and muscle.

found that Mo levels in all measured organs were not high even after only one day, despite substantial RES retention of Mo in liver and spleen, in which the Mo content also quickly decreased at later time points. Importantly, after 7 days, Mo levels in all measured organs became very low, demonstrating that MoOx-PEG could be excreted nearly completely from the mouse body. Furthermore, the urine and feces of mice were collected to study the metabolic pathway of MoOx-PEG (Figure 2b). High levels of Mo were detected in both urine and feces, particularly in the first 12 h, indicating that MoOx-PEG could be quickly excreted through both renal and fecal pathways. Importantly, it was also found that MoOx-PEG excreted neither in vitro cytotoxicity to different types of cell lines (Supporting Information, Figure S7), nor noticeable in vivo toxic effect to the treated mice within 15 days (dose = 20 mg kg^{-1}) (Supporting Information, Figures S8, S9). Considering the very little retention of remaining Mo-species in the mouse body after 15 days, it may be fair to predict that our MoOx-PEG nanosheets would not show any further long-term toxicity to mice at this dose.

A possible mechanism is proposed to explain such observed rapid clearance. Although MoOx-PEG upon intravenous injection would accumulate in RES organs, similar to the in vivo behaviors of other nanoparticles with sizes larger than 6–8 nm, the gradual oxidation of MoOx under normal physiological pH could lead to the decomposition of those nanosheets and possibly yield $[Mo^{VI}O_4]^{2-}$ ions or ultra-small nanoparticles, which are water-soluble and may be able to go through the kidney filtration. In the meanwhile, a certain proportion of decomposed Mo-species may also be excreted via the binary pathway into feces. Such a rapid excretion behavior has been rarely observed for typical inorganic nanomaterials with sizes larger than the kidney filtration threshold.

Being rather distinctive from the physiological environment in normal tissues, the tumor microenvironment is more acidic and usually has a lower oxygen level (hypoxia).[9] In particular, the pH inside 4T1 murine breast cancer tumors was measured to be 6.0–6.5 in our recent work.[15] We thus hypothesize that MoOx-PEG may show a slower degradation in the tumor compared to that in normal tissues. Because of the high NIR absorbance, MoOx-PEG is able to offer strong contrast under photoacoustic (PA) imaging. We therefore used PA imaging to monitor the in vivo degradation of MoOx-PEG in both muscles and tumors. Mice bearing 4T1 tumors were intratumorally (i.t.) or intramuscularly (i.m., on their thighs) injected with MoOx-PEG (0.2 mg mL^{-1}, 25 μL). PA imaging was conducted at both positions for mice right after injection of MoOx-PEG and 24 h post injection (Figure 2c,d). Interestingly, compared to PA signals in muscles in which only about 30% of their original signals were left 24 h later, largely retained PA signals were observed in the tumor after 24 h (ca. 60% of signals remained there), demonstrating the obviously slower degradation of MoOx-PEG in the tumor than that in the muscle. Such pH-dependent, organ-selective degradation behavior of MoOx-PEG would enable longer tumor retention of MoOx-PEG, particularly favorable for the applications in tumor-targeted imaging or therapy.

Next, we wondered whether those MoOx-PEG nanosheets could still target tumors by the EPR effect. PA imaging was employed to real-time monitor the tumor homing of those nanosheets after i.v. injection of MoOx-PEG (20 mg kg^{-1}) into 4T1 tumor-bearing mice (Figure 3a). The photoacoustic signals in the tumor region gradually increased within the first 6 h post injection, and remained at a high level even after 24 h, indicating the efficient tumor homing and retention of MoOx-PEG after systemic administration. Notably, although MoOx-PEG would gradually degrade within serum, it still showed a relatively long blood circulation time post i.v. injection (Supporting Information, Figure S10), favorable for tumor passive accumulation by the well-known EPR effect (Supporting Information, Figure S11).

Owing to the strong NIR absorption, MoOx-PEG (50 μg mL^{-1}) could efficiently kill 4T1 cancer cells under 808-nm laser irradiation (0.7 W c^{-2}, 6 min) in vitro (Supporting Information, Figure S12). With efficient tumor homing, i.v. injection of MoOx-PEG (dose = 20 mg kg^{-1}) could also lead to rapid heating of 4T1 tumors to about 55 °C within 10 min when the tumors on mice were exposed to the 808-nm laser at a power density of 0.7 W c^{-2} (Figure 3b). In contrast, the tumor injected with PBS showed little temperature increase under the same irradiation condition (Figure 3b). To evaluate the therapeutic efficacy, mice bearing 4T1 tumors were divided into five groups: (1) PBS; (2) NIR (laser only); (3) MoOx-PEG only (i. t. injection, 1.25 mg kg^{-1}); (4) MoOx-PEG (i.t. injection, 1.25 mg kg^{-1}) + laser, (5) MoOx-PEG laser (i.v. injection, 20 mg kg^{-1}) + laser. Laser irradiation (0.7 W c^{-2}, 10 min) was carried out either 0.5 h after i. t. injection or 6 h after i.v. injection of MoOx-PEG. As expected, tumors treated with MoOx-PEG (i.t. or i.v. injection) + laser irradiation (group 4 and 5) were completely

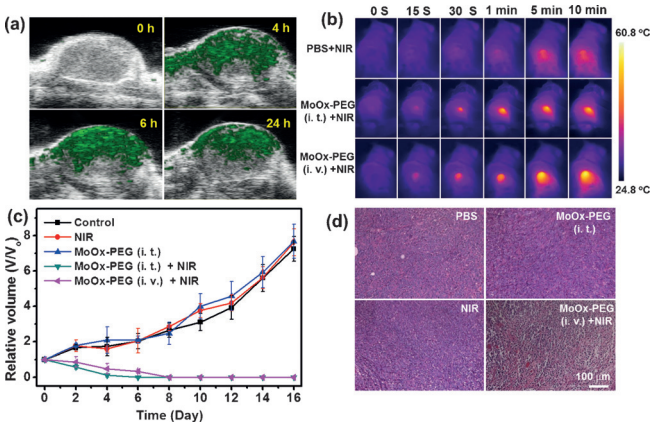

Figure 3. In vivo photothermal therapy. a) Overlaid US and PA imaging of tumors on mice taken at various time points after i.v. injection with MoOx-PEG. b) IR thermal images of 4T1 tumor-bearing mice, which were injected with MoOx-PEG and then exposed to the 808-nm laser ($0.7\ W\,c^{-2}$) for 10 min. c) The growth of 4T1 tumors in different groups of mice treated with PBS injection; laser only; MoOx-PEG (i.t.); MoOx-PEG (i.t.) + laser; MoOx-PEG (i.v.) + laser. d) Micrographs of H&E staining tumor slices collected from different groups as indicated. The doses of MoOx-PEG were fixed at $1.25\ mg\,kg^{-1}$ for i.t. injection and $20\ mg\,kg^{-1}$ for i.v. injection. Laser irradiation was conducted 30 min after i.t. injection and 24 h after i.v. injection of MoOx-PEG.

eliminated right after laser exposure, and showed no reoccurrence within 16 days (Figure 3c; Supporting Information, Figure S13). In contrast, neither laser irradiation only (group 2) nor MoOx-PEG injection (i.t.) (group 3) would affect the tumor growth. Furthermore, histological examination of tumors treated with MoOx-PEG (i.v. injection) + laser irradiation (group 5) showed obvious pyknosis, karyorrhexis, and karyolysis for all tumor cells, suggesting the highly effective photothermal ablation of cancer using MoOx-PEG (Figure 3d).

Two-dimensional nanostructures such as graphene and MoS_2 with rather large specific surface area have been widely exploited as drug carriers with high loading capacities.[5a,b] Considering the atomic-thin layered structure of MoOx-PEG nanosheets, we also tested its ability to load therapeutic molecules, including 7-Ethyl-10-hydroxycamptothecin (SN38, a chemotherapy drug), and chlorine e6 (Ce6, a photodynamic agent), by simply mixing MoOx-PEG with SN38 or Ce6 under pH 5.4. Excitingly, it was found that MoOx-PEG could effectively load both SN38 and Ce6, with the loading ratios ([drug]/ [MoOx], w/w) determined to be about 230% and about 80% (Table 1; Supporting Information, Figure S14), respectively, likely owing to the hydrophobic interaction between those therapeutic molecules and the nanosheet surface. Moreover, in vitro experiments further evidenced that those therapeutic molecules loaded on MoOx-PEG nanosheets showed retained (for SN38 in chemotherapy) or even improved (for Ce6 in photodynamic therapy) *anti*-cancer activities (Supporting Information, Figure S14c,f). Therefore, 2D MoOx-PEG nanosheets could also act as an effective drug carrier, potentially useful to realize combination therapy of cancer (for example, combining photothermal and photodynamic and chemotherapy for synergistic cancer treatment).

Table 1: Drug loading capacities for MoOx-PEG.

Drug	Added ratio (w/w) [Drug]/[MoOx]	Loaded ratio (w/w) [Drug]/[MoOx]
SN38	4:1	ca. 230
Ce6	4:1	ca. 80

In summary, we have developed a novel type of 2D nanomaterial, MoOx-PEG nanosheets, with pH-dependent decomposition behavior, strong NIR absorbance, and efficient drug loading capabilities. After intravenous injection, MoOx-PEG shows rapid clearance from normal organs of mice, but would accumulate in the tumor by the EPR effect and stay there for much longer, owing to the distinctive differences between the tumor microenvironment and normal physiological conditions. Apart being a rather robust photothermal agent to realize effective in vivo tumor ablation under NIR laser, MoOx-PEG can also act as a drug carrier to load various therapeutic molecules with high efficiencies. The NIR mass extinction coefficient and drug loading capacities of MoOx-PEG are found to be higher or comparable to those of other 2D nanomaterials commonly explored in cancer theranostics.[16] The rapid excretion, absence of in vivo long term toxicity, and efficient tumor passive retention abilities of MoOx-PEG further make it an attractive agent for in vivo applications. More importantly, our study develops a unique approach to achieve a long-term goal in nanomedicine research, particularly for the development of inorganic nanoagents; that is, to realize rapid body clearance and efficient tumor retention of nanoparticles at the same time, a seemingly easy aim but that can hardly be possible by simply tuning nanoparticle sizes and surface coatings. Such a strategy may be extended to design of other functional inorganic nanostructures for biomedical applications, and indicate that it would be of great importance to take the unique features of tumor microenvironment into account when designing cancer-targeted imaging or therapy agents.

Acknowledgements

This work was partially supported by the National Natural Science Foundation of China (51525203, 51302180, 51222203, 51472049), the National "973" Program of China (2011CB911002, 2012CB932601), a Project Funded by the Priority Academic Program Development of Jiangsu Higher Education Institutions, and the Post-doctoral science foundation of China (2014M561706).

Keywords: antitumor agents · molybdenum oxide · nanosheets · photothermal therapy · rapid clearance

How to cite: *Angew. Chem. Int. Ed.* **2016**, *55*, 2122–2126
Angew. Chem. **2016**, *128*, 2162–2166

[1] L. Cheng, C. Wang, L. Feng, K. Yang, Z. Liu, *Chem. Rev.* **2014**, *114*, 10869–10939.

[2] a) Y. Sun, W. Feng, P. Yang, C. Huang, F. Li, *Chem. Soc. Rev.* **2015**, *44*, 1509 – 1525; b) X. Li, X. Liu, D. M. Chevrier, X. Qin, X. Xie, S. Song, H. Zhang, P. Zhang, X. Liu, *Angew. Chem. Int. Ed.* **2015**, *54*, 13312 – 13317; *Angew. Chem.* **2015**, *127*, 13510 – 13515; c) X. Liang, Y. Li, X. Li, L. Jing, Z. Deng, X. Yue, C. Li, Z. Dai, *Adv. Funct. Mater.* **2015**, *25*, 1451 – 1462; d) X. Sun, W. Cai, X. Chen, *Acc. Chem. Res.* **2015**, *48*, 286 – 294.
[3] Q. He, J. Shi, *Adv. Mater.* **2014**, *26*, 391 – 411.
[4] a) G. Song, C. Liang, H. Gong, M. Li, X. Zheng, L. Cheng, K. Yang, X. Jiang, Z. Liu, *Adv. Mater.* **2015**, *27*, 6110 – 6117; b) Z. Sun, H. Xie, S. Tang, X.-F. Yu, Z. Guo, J. Shao, H. Zhang, H. Huang, H. Wang, P. K. Chu, *Angew. Chem. Int. Ed.* **2015**, *54*, 11526 – 11530; *Angew. Chem.* **2015**, *127*, 11688 – 11692; c) G. Song, Q. Wang, Y. Wang, G. Lv, C. Li, R. Zou, Z. Chen, Z. Qin, K. Huo, R. Hu, J. Hu, *Adv. Funct. Mater.* **2013**, *23*, 4281 – 4292.
[5] a) K. Yang, L. Feng, X. Shi, Z. Liu, *Chem. Soc. Rev.* **2013**, *42*, 530 – 547; b) T. Liu, C. Wang, X. Gu, H. Gong, L. Cheng, X. Shi, L. Feng, B. Sun, Z. Liu, *Adv. Mater.* **2014**, *26*, 3433 – 3440; c) J. Liu, M. Yu, C. Zhou, S. Yang, X. Ning, J. Zheng, *J. Am. Chem. Soc.* **2013**, *135*, 4978 – 4981.
[6] H. S. Choi, W. Liu, P. Misra, E. Tanaka, J. P. Zimmer, B. I. Ipe, M. G. Bawendi, J. V. Frangioni, *Nat. Biotechnol.* **2007**, *25*, 1165 – 1170.
[7] L. Guo, I. Panderi, D. D. Yan, K. Szulak, Y. Li, Y.-T. Chen, H. Ma, D. B. Niesen, N. Seeram, A. Ahmed, B. Yan, D. Pantazatos, W. Lu, *ACS Nano* **2013**, *7*, 8780 – 8793.
[8] a) S. Tang, M. Chen, N. Zheng, *Small* **2014**, *10*, 3139 – 3144; b) H. Xing, S. Zhang, W. Bu, X. Zheng, L. Wang, Q. Xiao, D. Ni, J. Zhang, L. Zhou, W. Peng, K. Zhao, Y. Hua, J. Shi, *Adv. Mater.* **2014**, *26*, 3867 – 3872; c) M. Zhou, J. Li, S. Liang, A. K. Sood, D. Liang, C. Li, *ACS Nano* **2015**, *9*, 7085 – 7096.
[9] X. Zheng, X. Wang, H. Mao, W. Wu, B. Liu, X. Jiang, *Nat. Commun.* **2015**, *6*, 5834.
[10] Q. Huang, S. Hu, J. Zhuang, X. Wang, *Chem. Eur. J.* **2012**, *18*, 15283 – 15287.
[11] a) M. Vasilopoulou, A. M. Douvas, D. G. Georgiadou, L. C. Palilis, S. Kennou, L. Sygellou, A. Soultati, I. Kostis, G. Papadimitropoulos, D. Davazoglou, P. Argitis, *J. Am. Chem. Soc.* **2012**, *134*, 16178 – 16187; b) M. M. Y. A. Alsaif, K. Latham, M. R. Field, D. D. Yao, N. V. Medehkar, G. A. Beane, R. B. Kaner, S. P. Russo, J. Z. Ou, K. Kalantar-zadeh, *Adv. Mater.* **2014**, *26*, 3931 – 3937.
[12] H. Cheng, T. Kamegawa, K. Mori, H. Yamashita, *Angew. Chem. Int. Ed.* **2014**, *53*, 2910 – 2914; *Angew. Chem.* **2014**, *126*, 2954 – 2958.
[13] J. T. Robinson, S. M. Tabakman, Y. Liang, H. Wang, H. Sanchez Casalongue, D. Vinh, H. Dai, *J. Am. Chem. Soc.* **2011**, *133*, 6825 – 6831.
[14] L. Cheng, J. Liu, X. Gu, H. Gong, X. Shi, T. Liu, C. Wang, X. Wang, G. Liu, H. Xing, W. Bu, B. Sun, Z. Liu, *Adv. Mater.* **2014**, *26*, 1886 – 1893.
[15] Q. Chen, X. Liu, J. Chen, J. Zeng, Z. Cheng, Z. Liu, *Adv. Mater.* **2015**, *27*, 6820 – 6827.
[16] Y. Chen, C. Tan, H. Zhang, L. Wang, *Chem. Soc. Rev.* **2015**, *44*, 2681 – 2701.

Received: November 16, 2015
Published online: December 28, 2015

